

PAPER

Frequency-dependent membrane polarization across neocortical cell types and subcellular elements by transcranial alternating current stimulation

To cite this article: Xuelin Huang *et al* 2024 *J. Neural Eng.* **21** 016034

View the [article online](#) for updates and enhancements.

You may also like

- [tACS facilitates flickering driving by boosting steady-state visual evoked potentials](#)
Bingchuan Liu, Xinyi Yan, Xiaogang Chen et al.
- [Responses of model cortical neurons to temporal interference stimulation and related transcranial alternating current stimulation modalities](#)
Boshuo Wang, Aman S Aberra, Warren M Grill et al.
- [Machine learning validation of EEG+tACS artefact removal](#)
Siddharth Kohli and Alexander J Casson

Breath Biopsy Conference

5th & 6th November
Online

Join the conference to explore the **latest challenges** and advances in **breath research**,
you could even **present your latest work!**

Register now for free!



Main talks



Early career sessions



Posters

Journal of Neural Engineering



PAPER

RECEIVED
17 October 2023

REVISED
29 January 2024

ACCEPTED FOR PUBLICATION
21 February 2024

PUBLISHED
29 February 2024

Frequency-dependent membrane polarization across neocortical cell types and subcellular elements by transcranial alternating current stimulation

Xuelin Huang, Xile Wei , Jiang Wang and Guosheng Yi*

School of Electrical and Information Engineering, Tianjin University, Tianjin 300072, People's Republic of China

* Author to whom any correspondence should be addressed.

E-mail: guoshengyi@tju.edu.cn

Keywords: transcranial alternating current stimulation (tACS), neocortical neurons, cell type, subcellular element, frequency-dependent membrane polarization

Supplementary material for this article is available [online](#)

Abstract

Objective. Transcranial alternating current stimulation (tACS) is a non-invasive brain stimulation technique that directly interacts with ongoing brain oscillations in a frequency-dependent manner. However, it remains largely unclear how the cellular effects of tACS vary between cell types and subcellular elements. **Approach.** In this study, we use a set of morphologically realistic models of neocortical neurons to simulate the cellular response to uniform oscillating electric fields (EFs). We systematically characterize the membrane polarization in the soma, axons, and dendrites with varying field directions, intensities, and frequencies. **Main results.** Pyramidal cells are more sensitive to axial EF that is roughly parallel to the cortical column, while interneurons are sensitive to axial EF and transverse EF that is tangent to the cortical surface. Membrane polarization in each subcellular element increases linearly with EF intensity, and its slope, i.e. polarization length, highly depends on the stimulation frequency. At each frequency, pyramidal cells are more polarized than interneurons. Axons usually experience the highest polarization, followed by the dendrites and soma. Moreover, a visible frequency resonance presents in the apical dendrites of pyramidal cells, while the other subcellular elements primarily exhibit low-pass filtering properties. In contrast, each subcellular element of interneurons exhibits complex frequency-dependent polarization. Polarization phase in each subcellular element of cortical neurons lags that of field and exhibits high-pass filtering properties. These results demonstrate that the membrane polarization is not only frequency-dependent, but also cell type- and subcellular element-specific. Through relating effective length and ion mechanism with polarization, we emphasize the crucial role of cell morphology and biophysics in determining the frequency-dependent membrane polarization. **Significance.** Our findings highlight the diverse polarization patterns across cell types as well as subcellular elements, which provide some insights into the tACS cellular effects and should be considered when understanding the neural spiking activity by tACS.

1. Introduction

Transcranial alternating current stimulation (tACS) is a non-invasive neuromodulation method that can modulate neural activity and brain behavior in a frequency-specific manner [1–4], thereby allowing study of causal links between brain oscillations and specific aspects of behavior [5–8]. There is also growing evidence that tACS has excellent potential as a

low-cost clinical tool in treating neurological and psychiatric disorders [4]. Despite its increasing interest, the efficacy of tACS is being questioned due to high variability of the induced effects [2, 9–11], which is attributed to the incomplete insights into tACS mechanisms. Instead of generating action potentials, tACS causes rhythmic fluctuations in the membrane voltage of neurons [12]. This subthreshold polarization leads to changes in spike timing [3, 13, 14]

and neural oscillations [4]. Therefore, characterizing the membrane polarization between neocortical cell types and subcellular elements systematically is of great significance for a comprehensive understanding of the cellular mechanisms of tACS.

By applying low-intensity sinusoidal currents through scalp electrodes, tACS generates a weak oscillating electric field (EF) in the targeted brain area, which induces transient membrane de- or hyperpolarization at the applied stimulation frequency [15, 16]. *In vitro* experiment [17] and modeling studies [15, 18] have shown that the tACS-induced membrane response in morphologically realistic cortical pyramidal cells is subthreshold and strongly depends on the stimulation frequency. Some modeling studies [15, 16, 18] indicate the significant difference in frequency-dependent membrane polarization between subcellular categories, which is affected by cell morphologies and active ion currents. Nevertheless, neuronal morphology and biophysics are substantially different between cortical cell types within the same species [19, 20]. Several works [21, 22] have considered some cortical neurons with distinct cell classes and quantify their somatic polarization during weak oscillating EF stimulation with a fixed frequency to understand the field entrainment of spiking activity. Although growing studies have investigated the membrane polarization by tACS, how the frequency-dependent polarization varies between neocortical neurons and their subcellular categories is still not fully understood. This poor understanding of the cellular mechanisms of tACS has hampered its scientific and clinical applications in regulating brain oscillations and related cognitive behavior.

The objective of this study is to examine how membrane polarization varies between cell types and subcellular elements (soma, axons, and dendrites) with weak oscillating EF stimulation. We use a set of conductance-based neocortical neuron models with realistic morphologies to simulate the cellular response over a range of stimulation parameters. Our results show that the membrane polarization is sensitive to field direction, intensity, and frequency. Moreover, the frequency-dependent polarization varies between cell types and subcellular elements, which is modulated by cell morphology and biophysics. These findings highlight the complex polarization patterns across cell types as well as subcellular categories, which should be considered when understanding the neural spiking activities and brain oscillations during tACS.

2. Models and methods

2.1. Neocortical neuron models

We adopt a set of modified versions of multi-compartmental, conductance-based neocortical neuron models originally released by the Blue Brain

Project [23, 24]. These models are modified to adapt the biophysical and geometric properties of adult, human cortical neurons, and their responses to sub-threshold stimulation with exogenous EF are validated based on *in vitro* measurements [19, 25]. Each modified model includes 3D reconstructed dendritic and axonal ramifications, with up to 13 different Hodgkin-Huxley-like ion channels distributed in the soma, axon initial segment, apical dendrites, and basal dendrites. This model set contains 5 cell types across all 6 neocortical layers, which are: layer 1 neurogliaform cell (L1 NGC), layer 2/3 pyramidal cell (L2/3 PC), layer 4 large basket cell (L4 LBC), layer 5 pyramidal cell (L5 PC) and layer 6 pyramidal cell (L6 PC). Each cell type is composed of five clone neurons with stochastic variations in their dendritic and axonal geometries to reflect morphological diversity within cell type. More model details are outlined in previous publications [19, 22], and the model set used in this paper can be downloaded from Tran's work [22]. Figure 1(a) depicts the morphologies of 25 modified neurons across 6 neocortical layers, in which the soma, axons, basal dendrites, and apical dendrites are colored by black, red, green, and blue, respectively.

2.2. Modeling of tACS

By applying sinusoidal currents through the stimulation electrodes attached to the scalp, tACS generates a subthreshold oscillating EF in the targeted brain area, which periodically de- and hyperpolarizes the membrane voltage of neurons. Despite its non-uniformly spatial distribution in brain tissues, the generating exogenous EF can be assumed to be uniformly distributed at the small scale of the neuron [22]. Therefore, the uniform oscillating EF is used to model the tACS effects at the cellular level, which is:

$$|\vec{E}| = A_E \sin(2\pi f_E t) \quad (1)$$

where \vec{E} is the field vector, A_E (mV mm^{-1}) and f_E (Hz) are the field intensity and frequency, respectively. Figure 1(b) shows the coordinate system for example model neuron (L5 PC, clone 4), with its somato-dendritic axis aligned to z -axis. The soma is placed at the origin. EF direction is given by polar angle θ_E (0° – 180°) and azimuthal angle φ_E (0° – 360°) with respect to the somato-dendritic axis in spherical coordinates. Indeed, the exogenous EF interacts with the cellular activities through changing the extracellular potentials of neurons. For the example model neuron in coordinate systems (figure 1(b)), the extracellular potential V_e at each compartment with position (x, y, z) is calculated by:

$$V_e(x, y, z) = -|\vec{E}| \cdot (x \sin \theta_E \cos \varphi_E + y \sin \theta_E \sin \varphi_E + z \cos \theta_E). \quad (2)$$

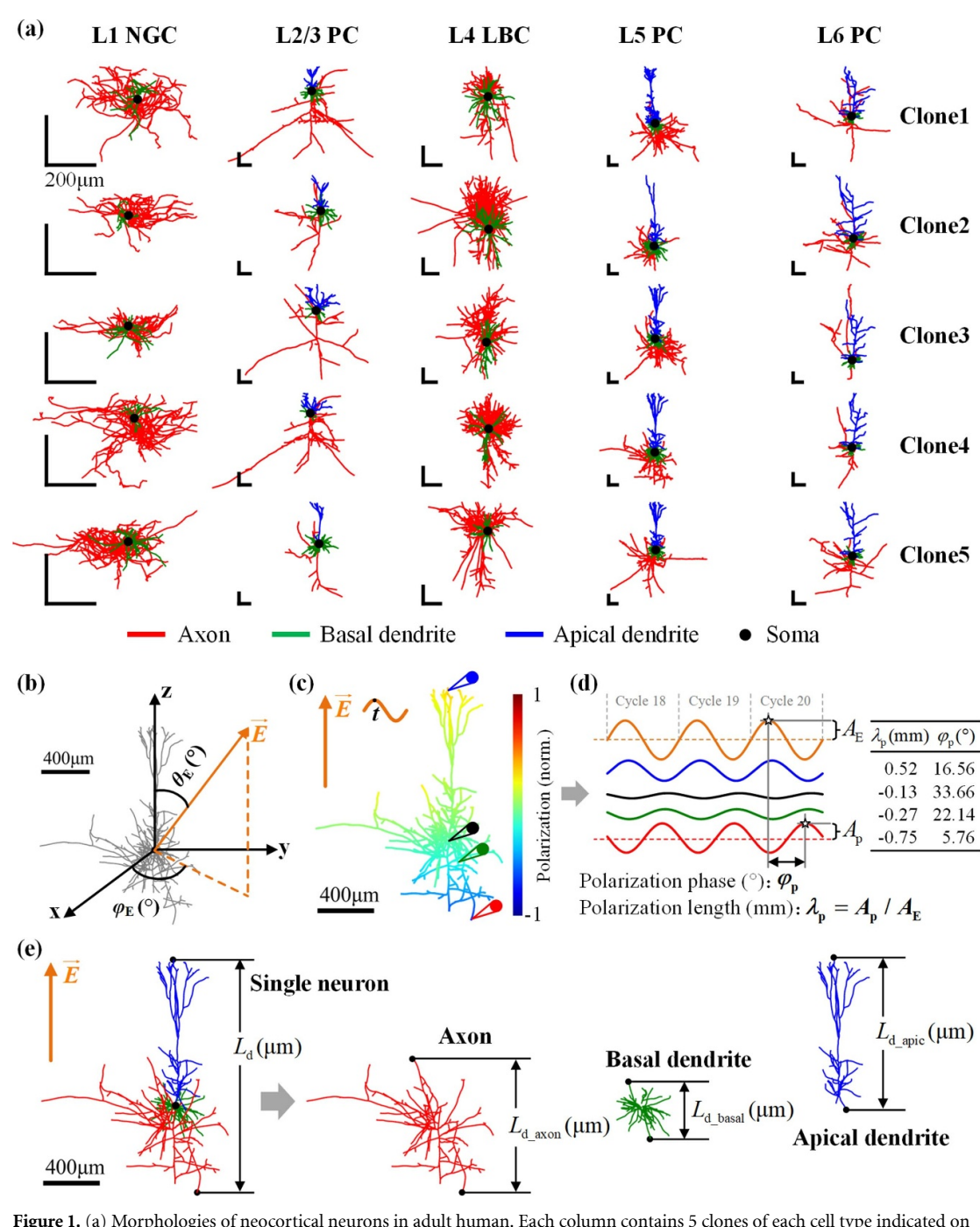


Figure 1. (a) Morphologies of neocortical neurons in adult human. Each column contains 5 clones of each cell type indicated on the top. Cell type abbreviations defined in section 2.1. Soma, axons, apical dendrites, and basal dendrites are colored by black, red, blue, and green respectively. Scale bars = 200 μm . (b) Coordinate system shown for example model neuron (L5 PC, clone 4), with its somato-dendritic axis aligned to z -axis. Electric field direction controlled by polar angle θ_E and azimuthal angle φ_E . (c) Normalized membrane polarization in example neuron by uniform oscillating fields with 1 mV mm^{-1} and 10 Hz at time t . Field direction indicated by $\theta_E = 0^\circ$ and $\varphi_E = 0^\circ$. (d) Field waveform and the resulting membrane voltage response in each subcellular element of the last three cycles, as well as the schematic of calculation of polarization length λ_p and polarization phase φ_p . Recording compartments as indicated in (c). (e) Schematic of effective polarization length L_d that reflects the maximum projection distance of cell morphology along the field direction, as well as the axonal effective length L_{d_axon} , basal dendritic effective length L_{d_basal} , and apical dendritic effective length L_{d_apic} .

The potential at the origin (soma) is set to zero [19, 26]. For pyramidal cells, we define the axial field that is roughly parallel to the cortical column ($0^\circ \leq \theta_E \leq 60^\circ$, $120^\circ < \theta_E \leq 180^\circ$) and transverse field that is tangent to the cortical surface ($60^\circ < \theta_E \leq 120^\circ$), due to their well-defined somato-dendritic

axis. However, given that the interneurons are more symmetric in shape and do not have a well-defined axis, we define the field orientation by considering their alignment with the cortical columns. According to [26], we define the upward EF with $0^\circ \leq \theta_E \leq 60^\circ$, which is analogous to field directed outward relative

to the cortical surface. We also define the downward field with $120^\circ < \theta_E \leq 180^\circ$, which is analogous to field directed inward relative to the cortical surface. Similarly, we define the transverse field with $60^\circ < \theta_E \leq 120^\circ$, which is analogous to field tangential to the cortical surface. Note that the axial field includes the upward field and downward field.

2.3. Calculations of polarization length and polarization phase

When a neuron is subjected to an EF, the branches at one end of the neuron are depolarized while the branches at the other end are hyperpolarized (figure 1(c)). Such de- or hyperpolarization follows the temporal pattern of the applied EF at the same frequency. We first compute the maximum membrane voltage deflection A_p (mV) [15, 16] by subtracting the resting potential of each compartment in the absence of stimulation from the corresponding peak voltage in the steady state under stimulation (figure 1(d)). The maximum membrane potential deflection varies between compartments. The axonal or apical dendritic compartment close to the anode or cathode tends to be more polarized, while the somatic or basal dendritic compartment experiences the smaller polarization. Furthermore, we use the polarization length λ_p [20, 22], an indicator of polarization per unit subthreshold field applied, to quantify the polarization sensitivity to oscillating field, which is computed by:

$$\lambda_p = A_p / A_E. \quad (3)$$

The unit of polarization length λ_p is millimeter (mm). Positive polarization length indicates a depolarization at the beginning of the positive half-circle EF, whereas a negative value indicates a hyperpolarization [20]. Such as, when undergoing an oscillating EF parallel to the positive z-axis, the polarization length in the apical dendrites of L5 PC clone 4 is positive, while the polarization length in the soma, axons, and basal dendrites is negative (figure 1(d), right table). Moreover, we compute the polarization phase φ_p ($^\circ$) based on the neuronal response of the last cycle. φ_p is the difference between the phase corresponding to the peak response of each compartment and the field phase that peak value occurs. Polarization phase φ_p always lags that of the applied field. In the case of a negative polarization length, the additional 180 degree phase difference should be removed for that it is reflected in the sign of the polarization length. Therefore, φ_p ranges between 0 and 180 degrees.

2.4. Morphologies and biophysics of neurons

Neuronal intrinsic properties, including morphologies and biophysics, play important roles in the subthreshold response to tACS [16, 18]. Here, we perform a quantitative analysis of the neuron

morphology and biophysics. We use the effective polarization length L_d (μm) to quantify the cell morphology [22], which is the distance between the two furthest compartments along the field direction (figure 1(e), left panel). A large L_d means that a neuron has a morphology specifically oriented in that axis. Furthermore, given the specific spatially distributed morphologies of non-soma subcellular elements, we quantify the axonal effective length L_{d_axon} , basal dendritic effective length L_{d_basal} , and apical dendritic effective length L_{d_apic} (figure 1(e), middle and right panels), which correspond to the maximum projection distances of the axons, basal dendrites, and apical dendrites along the field direction, respectively. In addition, we perform two control simulations to study the effect of biophysics on membrane polarization. One control simulation is to set all the cell dynamics to the same excitatory dynamics in L5 PCs, while the other is to set all the cell dynamics to the same inhibitory dynamics in L4 LBCs [22]. Under the control simulation, all 25 cells have the same ion channel types and distributions.

2.5. Simulations

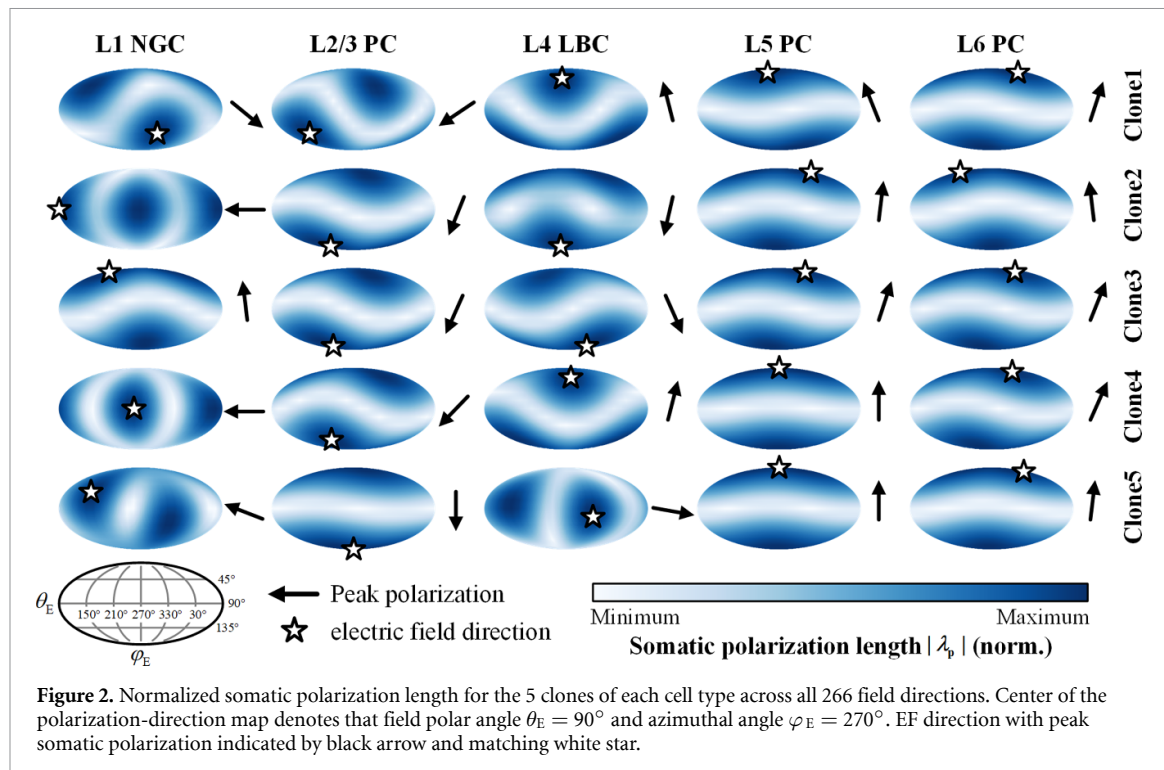
All the neuron modeling and tACS stimulation are implemented in the NEURON environment (v8.2.0) [27] with a time step of 25 μs . NEURON stimulation control, data analysis, and visualization are conducted in Matlab R2022a. EF intensity A_E is varied from 0.1 mV mm $^{-1}$ to 3 mV mm $^{-1}$ at a step size of 0.1 mV mm $^{-1}$. EF frequency f_E is varied from 1 Hz to 100 Hz at a step size of 1 Hz. Without specific instruction, the default values of A_E and f_E are 1 mV mm $^{-1}$ and 10 Hz, respectively. EF polar angle θ_E ranges from 0° to 180° in steps of 15° and azimuthal angle φ_E ranges from 0° to 360° in steps of 15° , resulting in 266 directions in total. Each simulation is performed no less than 20 stimulation cycles to avoid the onset transients and to reach the steady-state oscillations, where the last-cycle response is used to calculate the polarization length and polarization phase.

Given that non-soma subcellular elements consist of multiple compartments, the results are obtained from one compartment (and the same compartment for each cell) among the same subcellular category with the maximum polarization at a given field direction. For consistency, we determine the recording compartment for subcellular elements other than the soma at a specific field direction as the same with the situation of 10 Hz and 1 mV mm $^{-1}$ EFs.

3. Results

3.1. Polarization sensitivity to EF direction

Earlier studies [15, 26] have shown that the membrane polarization of neurons is sensitivity to the direction of applied EFs. In the presence of uniform oscillating EFs, we first quantify the somatic



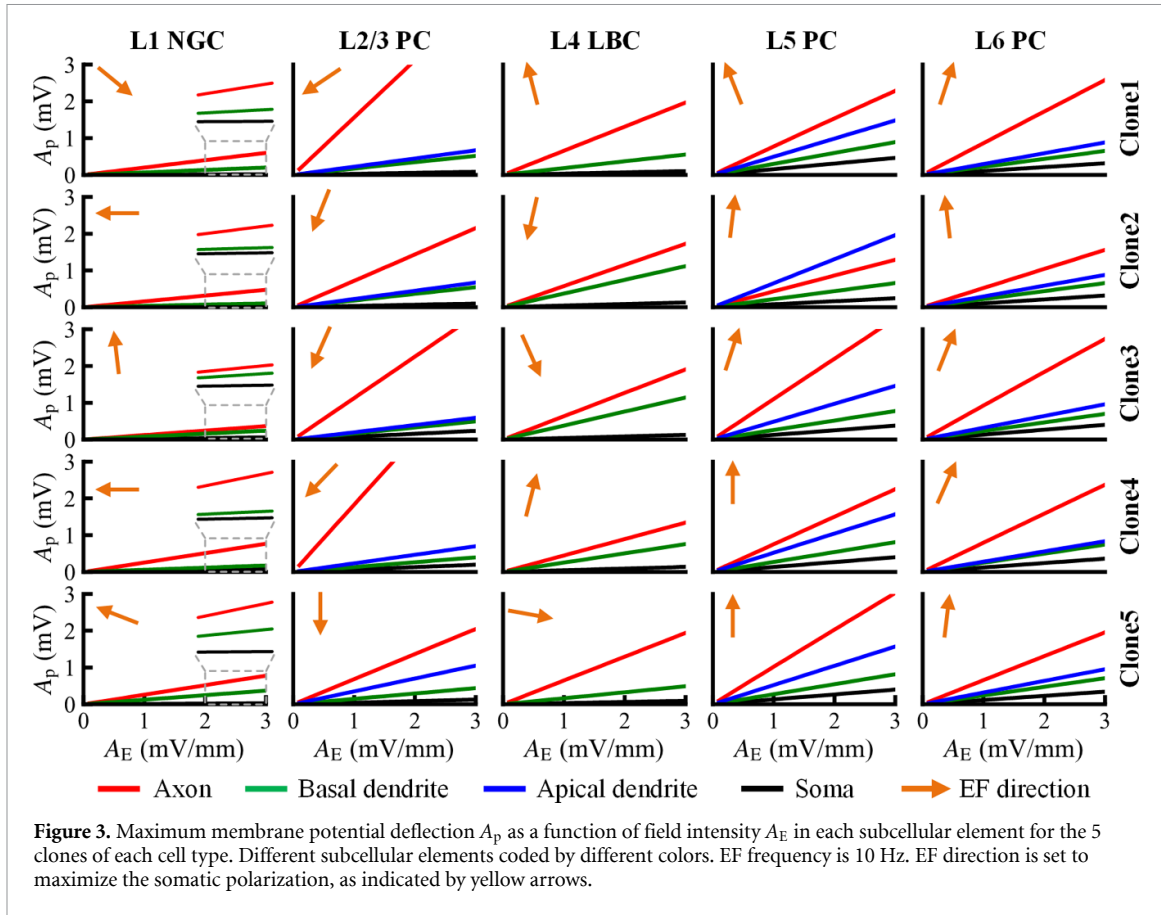
polarization of 25 clones spanning 6 neocortical layers across the full range of possible field directions. EF intensity and frequency are 1 mV mm^{-1} and 10 Hz, respectively. EF direction is controlled through spanning the polar and azimuthal angles in steps of 15° , totaling 266 directions. The induced somatic polarization is distributed spherically, which is normalized and projected into polarization-direction map (figure 2) using the Mollweide projection. In figure 2, the schematic of field polar angle θ_E and azimuthal angle φ_E is indicated by the subplot in the lower left corner. The arrow and star represent the optimal EF direction that a neuron experiences its peak somatic polarization.

We find that the somatic polarization of each cell is sensitive to the field direction. For pyramidal cells, L2/3 PCs experience their peak somatic polarization with downward EF ($120^\circ < \theta_E \leq 180^\circ$), while L5 and L6 PCs experience their peak somatic polarization with upward EF ($0^\circ \leq \theta_E \leq 60^\circ$). In these cells, the polarization in the soma follows a smooth parabolic dependency on the polar angle, with little variation due to azimuthal rotations of the field. However, the somatic polarization sensitivity in interneurons to field direction varies between clones within the same cell type. Clone 3 of L1 NGCs and clones 1, 4 of L4 LBCs experience the maximum somatic polarization for upward field, while clone 1 of L1 NGCs and clones 2, 3 of L4 LBCs have the peak somatic polarization with downward field. The somatic polarization of the other interneuron clones is more sensitive to transverse field ($60^\circ < \theta_E \leq 120^\circ$). Compared to pyramidal cells, the somatic polarization of interneurons is

affected not only by the polar angle but also by the azimuthal angle of the applied field.

Furthermore, we quantify the peak polarization in the axons, basal dendrites, and apical dendrites of excitatory and inhibitory cells across 266 field directions. Note that the results in figure S1 are obtained from one compartment among the same subcellular category with the maximum polarization at a specific field direction. We find that the axons of L1 NGCs experience the peak polarization with transverse field due to their elongated axonal branches in the tangential direction of the cortex (figure S1(a)). However, the axonal polarization in most cells of the other cortical layers has the maximum value for axial field, while the axonal polarization in clones 2, 3 of L4 LBCs, clones 2, 4 of L5 PCs, and clone 2 of L6 PCs has the peak value for transverse field. Basal dendrites in most cells tend to be more polarized by axial field, while the basal dendrites in clones 3, 4, 5 of L1 NGCs and clone 1 of L2/3 PCs experience the maximum polarization for transverse field (figure S1(b)). Moreover, the polarization in the apical dendrites of clones 3 and 4 of L2/3 PCs is more sensitive to transverse field, whereas the apical dendrites in the other pyramidal cells exhibit directional sensitivity similar to the soma (figure S1(c)), potentially due to the slender apical tuft along the somato-dendritic axis.

These findings demonstrate that the polarization sensitivity to EF direction varies between cell types and subcellular elements. Moreover, the optimal field direction with peak axonal or apical dendritic polarization can be explained, to some extent, by the direction with the farthest morphological distribution of



relevant subcellular element. In summary, pyramidal cells are more sensitive to axial EF, while interneurons are sensitive not only to axial EF but also to transverse EF.

3.2. Polarization sensitivity to EF intensity

Previous studies [16, 17] demonstrate that the relation between applied oscillating EF intensity and resulting changes in transmembrane potential of neurons is linear. Here, we quantify the maximum membrane potential deflection A_p in each subcellular element of each cell over a range of field intensities. EF intensity is varied from 0.1 mV mm^{-1} to 3 mV mm^{-1} at a step size of 0.1 mV mm^{-1} . EF frequency is 10 Hz. EF direction is set to maximize the somatic polarization, as indicated in figure 2. For non-soma subcellular elements, the results are obtained from one compartment (and the same compartment for each cell) among the same subcellular category with the maximum polarization, same as below.

As depicted in figure 3, the maximum membrane potential deflection in each subcellular element of each neuron increases linearly with field intensity. Despite applying the optimal field direction for cell soma, the soma in each cell experiences the lowest polarization compared to the axons and dendrites. Axonal polarization is greater than that of dendrites for most cortical cells, with the exception of clone 2 in

L5 PCs that its peak polarization in the apical dendrites is higher than its axonal polarization. Moreover, the apical dendrites of pyramidal cells are more polarized compared to basal dendrites. The slope of each $A_p - A_E$ relationship, i.e. amplitude of polarization length $|\lambda_p|$, is constant. Nevertheless, the polarization length is highly variable across cell types as well as subcellular elements.

Figure 4 summarizes the polarization length λ_p for the 5 clones of each cell type, grouped by layer, in the soma, axons, basal dendrites, and apical dendrites based on figure 3. The filled geometry indicates a positive polarization length, while the unfilled geometry indicates a negative polarization length. We find that the soma, axons, and basal dendrites in L2/3 PCs have the positive polarization length, while their apical dendrites have the negative polarization length. In contrast, the polarization length in the soma, axons, and basal dendrites of L5 and L6 PCs is negative, while the polarization length in the apical dendrites is positive. For interneurons, the somatic polarization length in L1 NGCs is negative, but positive in L4 LBCs. However, the polarization length in the axons or basal dendrites consists of positive and negative values due to the heterogeneous sensitivity to the field direction between clones.

Moreover, L5 and L6 PCs experience the highest somatic polarization ($0.08\text{--}0.16 \text{ mm}$, $0.11\text{--}0.13 \text{ mm}$),

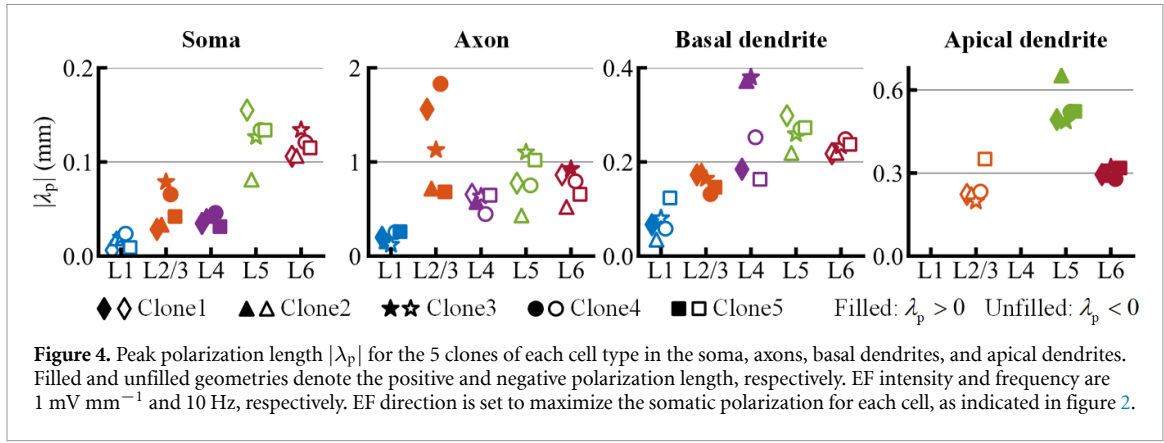


Figure 4. Peak polarization length $|\lambda_p|$ for the 5 clones of each cell type in the soma, axons, basal dendrites, and apical dendrites. Filled and unfilled geometries denote the positive and negative polarization length, respectively. EF intensity and frequency are 1 mV mm^{-1} and 10 Hz , respectively. EF direction is set to maximize the somatic polarization for each cell, as indicated in figure 2.

followed by L2/3 PCs (0.03–0.08 mm), L4 LBCs (0.03–0.05 mm), and L1 NGCs (0.01–0.02 mm). L2/3 PCs have the higher axonal polarization (0.68–1.83 mm) than L5 PCs (0.43–1.10 mm), L6 PCs (0.52–0.93 mm), and L4 LBCs (0.45–0.66 mm), while L1 NGCs have the lowest axonal polarization (0.12–0.26 mm). Basal dendrites in L4 LBCs are more polarized (0.16–0.38 mm), followed by L5 PCs (0.22–0.30 mm), L6 PCs (0.22–0.25 mm), L2/3 PCs (0.13–0.18 mm), and L1 NGCs (0.04–0.12 mm). As for the apical dendrites in excitatory cells, the highest polarization occurs in L5 PCs (0.49–0.65 mm), followed by L6 PCs (0.28–0.32 mm) and L2/3 PCs (0.20–0.35 mm). In summary, the pyramidal cells tend to be more polarized than interneurons. For excitatory neurons, L5 PCs usually experience the highest polarization, followed by L6 PCs and L2/3 PCs. Note that the axons in L2/3 PCs experience the highest polarization. For interneurons, the polarization in each subcellular element of L4 LBCs is always greater than that of L1 NGCs.

Given that the non-soma subcellular elements have their maximum polarization length for a particular orientation, we also simulate the results with the field direction that maximizes the axonal, basal dendritic, or apical dendritic polarization, respectively (figures S2(a)–(c)). As we expected, changing the field direction results in changes in polarization length, including its amplitude and sign. Especially, we find that the non-axon subcellular elements in interneurons, L5 and L6 PCs, experience the smallest polarization with the field direction that maximizes the axonal polarization (figure S2(d), red cycles). Above results indicate that the membrane polarization of neurons is linearly correlated to EF intensity at a fixed frequency, and such field sensitivity varies prominently between cell types and subcellular elements.

3.3. Polarization sensitivity to EF frequency

Evidence suggests that the amplitude and phase of membrane polarization both are highly frequency-dependent [16, 18]. Here, we quantify the

polarization length as well as polarization phase over a range of stimulation frequencies to examine the dependence of membrane polarization on field frequency across cell types and subcellular elements. EF frequency is varied from 1 Hz to 100 Hz at a step size of 1 Hz. EF intensity is 1 mV mm^{-1} , and EF direction is set to the optimal field orientation for soma indicated by figure 2.

As shown in figure 5, the peak polarization length in each subcellular element of 25 cells strongly depends on the stimulation frequency. Within the frequency range considered, the axons experience the highest polarization, followed by dendrites, while the soma experiences the lowest polarization. Note that the apical dendritic polarization in clone 2 of L5 PCs is higher than its axonal polarization at low frequencies (<40 Hz), potentially due to its compact morphology distribution of axons that results in a lower axonal polarization. For interneurons, the polarization in the soma and axons of interneurons exhibits complex filtering properties, including low-pass, band-pass, and high-pass filtering, while the polarization in the basal dendrites primarily shows the low-pass filtering properties (figure S3). On the contrary, the polarization in the soma, axons, and basal dendrites in most pyramidal cells decreases with field frequency. Soma in clones 1, 3, 4 of L2/3 PCs and axons in clone 3 of L6 PCs exhibit band-pass filtering properties. For excitatory neurons, the apical dendrites of L5 PCs are more polarized than their basal dendrites at each frequency. The polarization length in the apical dendrites of L2/3 and L6 PCs is higher than that of basal dendrites at low frequencies, with opposite effects at high frequencies. Moreover, there is a visible frequency resonance in the membrane polarization of apical dendrites for pyramidal cells, with the resonance frequency ranging between 4 Hz and 12 Hz.

Furthermore, we find that the polarization phase φ_p is also highly dependent on EF frequency. The polarization phase in each subcellular element of neocortical cells always lags that of the field, i.e. >0 , and increases with the field frequency (figure 6). For inhibitory neurons, the somatic polarization phase in

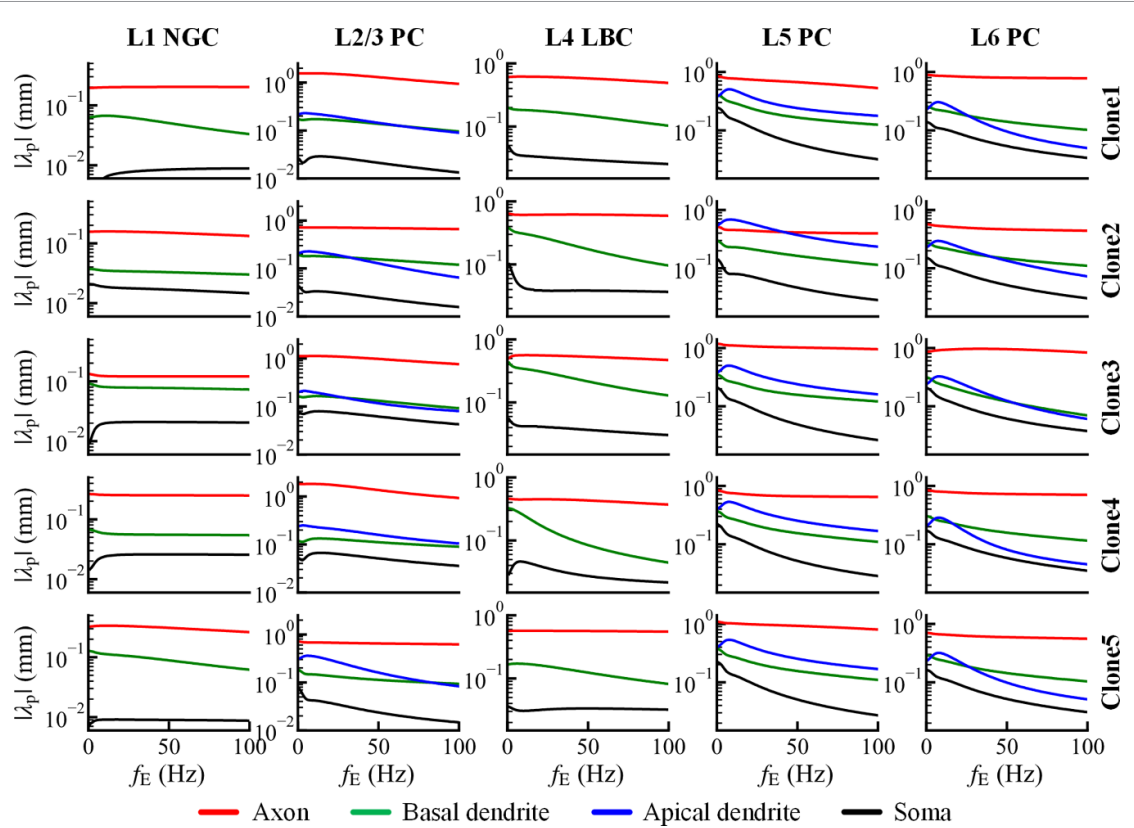


Figure 5. Peak polarization length $|\lambda_p|$ as a function of EF frequency f_E in each subcellular element (color-coded) of each cell. EF intensity is 1 mV mm^{-1} . EF direction is set to maximize the somatic polarization for each cell, as indicated in figure 2.

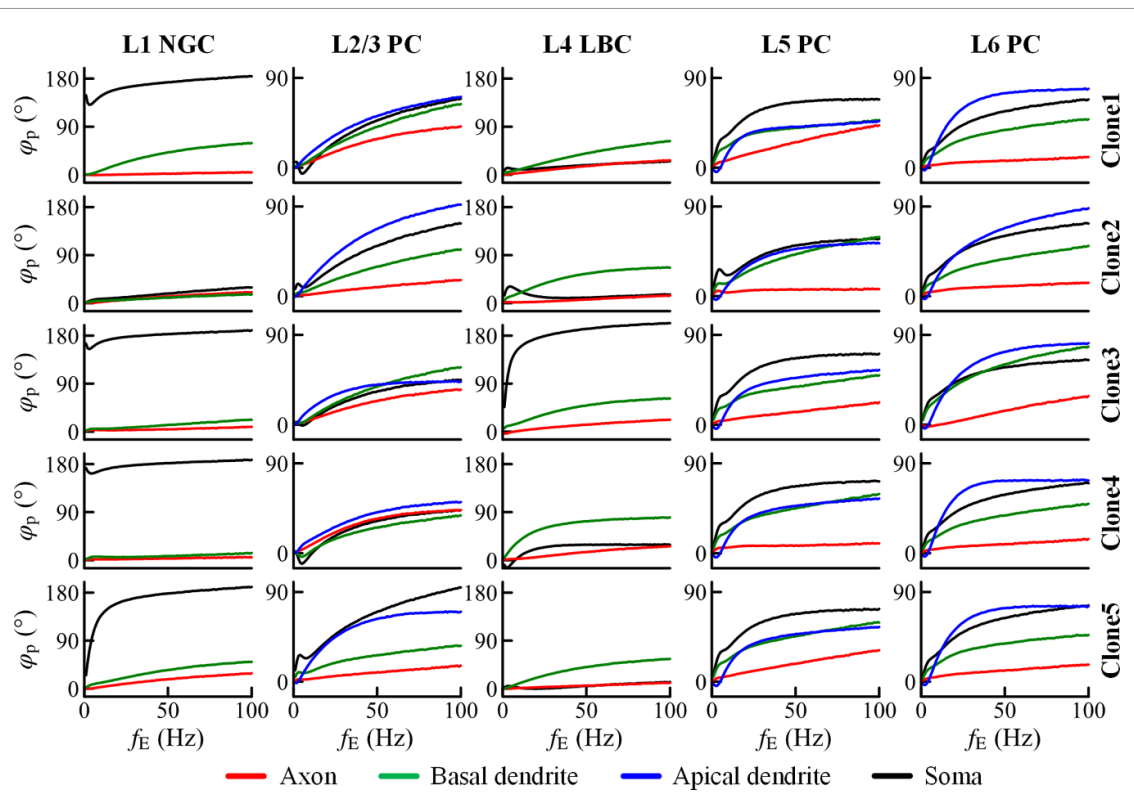


Figure 6. Polarization phase φ_p as a function of EF frequency f_E in each subcellular element (color-coded) of each cell. EF intensity is 1 mV mm^{-1} . EF direction is set to maximize the somatic polarization for each cell, as indicated in figure 2.

clones 1, 3, 4 of L1 NGCs is close to 180 degrees, while in clone 5 of L1 NGCs and clone 3 of L4 LBCs increases significantly with field frequency. The somatic polarization phase in the other interneurons is close to zero and changes a little with varying field frequencies. Axons of each interneuron have the smallest polarization phase that is less sensitivity to field frequency, whereas the polarization phase in the basal dendrites increases moderately with field frequency. For pyramidal neurons, the polarization phase in each subcellular element is also sensitive to field frequency and is less than 90 degrees within the frequency range considered. The polarization phase in the axons is lower than that of other subcellular elements and increases slowly with field frequency, while the polarization phase in the basal dendrites increases moderately with field frequency. The polarization phase in the soma and apical dendrites increases rapidly with field frequency and then become saturated. These findings show that the membrane polarization is strongly frequency-dependent, which varies between cell types as well as subcellular elements, suggesting that the cellular effects of tACS are highly variable.

3.4. Effects of cell morphology and biophysics on the membrane polarization

Earlier studies [16, 18] have identified the important role of cell morphology in modulating the membrane polarization induced by weak oscillating EFs. In order to quantify the morphology for each neuron, we compute the effective length L_d that is the distance from the two distal ends of a neuron in the field direction. Here, we investigate the relation between the polarization length and the effective length L_d for the 5 clones of each cell type across 266 field directions, totaling 5×266 data points. EF intensity and frequency are 1 mV mm^{-1} and 10 Hz, respectively. At each field orientation, the results of non-soma subcellular elements are obtained from one compartment among the same subcellular category with the maximum polarization length. Note that the recording compartments may be different with varying field directions.

For excitatory and inhibitory cells, the peak polarization length in the axons and entire neuron is highly correlated to the effective length ($R^2 > 0.9$ for L1 NGCs and L2/3 PCs, > 0.8 for L4 LBCs, > 0.7 for L5 and L6 PCs, figure 7(a)). Somatic and dendritic polarizations are poorly related to the effective length for interneurons and L2/3 PCs ($R^2 < 0.1$), but moderately related to the effective length for L5 and L6 PCs ($R^2 > 0.45$). Furthermore, we find that such relationship varies significantly between clones within the same cell type (figure 7(b)). For example, the correlation coefficient R^2 in the soma of L2/3 PCs varies between 0.04 and 0.71, while the R^2 in the apical dendrites varies between 0.03 and 0.80. Given that the specific morphology distribution of non-soma

subcellular elements, we compute the subcellular effective length for the axons L_{d_axon} , basal dendrites L_{d_basal} , and apical dendrites L_{d_apic} , which reflect their maximum projection distance along the field direction. We then study the relation between polarization length for each subcellular element and its effective length (figure S4). We find the obviously enhanced correlation in the basal dendrites for L1 NGCs, L2/3 PCs, L4 LBCs, and in the apical dendrites for excitatory cell types (figure S4(a)). Nevertheless, the correlation in the basal dendrites of L5 and L6 PCs becomes extremely weak. Similarly, the R^2 also varies between clones within the same cell type significantly (figure S4(b)).

Above results show that the axonal polarization of each cell type is determined by the cell morphology to a large extent. The similar polarization distribution between axons and entire neuron indicates that the neuronal peak polarization primarily occurs at the axonal terminals. Moreover, the polarization in the soma and dendrites of pyramidal cells could be partially predicted by cell morphologies, while the peak polarization of non-soma subcellular elements of cortical neurons could be well predicted by their respective subcellular morphologies.

In addition, there is evidence that cell biophysics is critical for modulating the response of neurons to oscillating EFs [16, 22]. Here, we make all cells have the same biophysics, i.e., the same ion channel types and distributions, to study the effects of biophysics on the frequency-dependent membrane polarization. EF intensity and frequency are 1 mV mm^{-1} and 10 Hz, respectively. EF direction is set to maximize the somatic polarization for each cell, as indicated in figure 2.

At first, we set all the cells dynamics to the same L5 excitatory dynamics. As shown in figure 8, L5 excitatory dynamics weakens the polarization in each subcellular element of inhibitory neurons, with little influence on the polarization in clone 3 of L4 LBCs. For excitatory neurons, L5 excitatory dynamics slightly attenuates the axonal polarization of L2/3 PCs but enhances the axonal polarization of L6 PCs, with little effect on the polarization in the soma and dendrites of L2/3 and L6 PCs. Moreover, L5 excitatory dynamics slightly decreases the polarization phase in each subcellular element of interneurons, with little influence on the polarization phase of L2/3 and L6 PCs (figure S5). Note that the changes in somatic polarization phase of clones 1, 3, 4, 5 of L1 NGCs are quite complex. Secondly, we set all the cells dynamics to the same L4 inhibitory dynamics. As shown in figure 9, L4 inhibitory dynamics slightly weakens the polarization in the axons but slightly strengthens the polarization in the other subcellular elements for L2/3 PCs. Each subcellular element of L5 and L6 PCs is more polarized compared to default dynamics. Particularly, L4 inhibitory dynamics decreases the resonance frequency of polarization

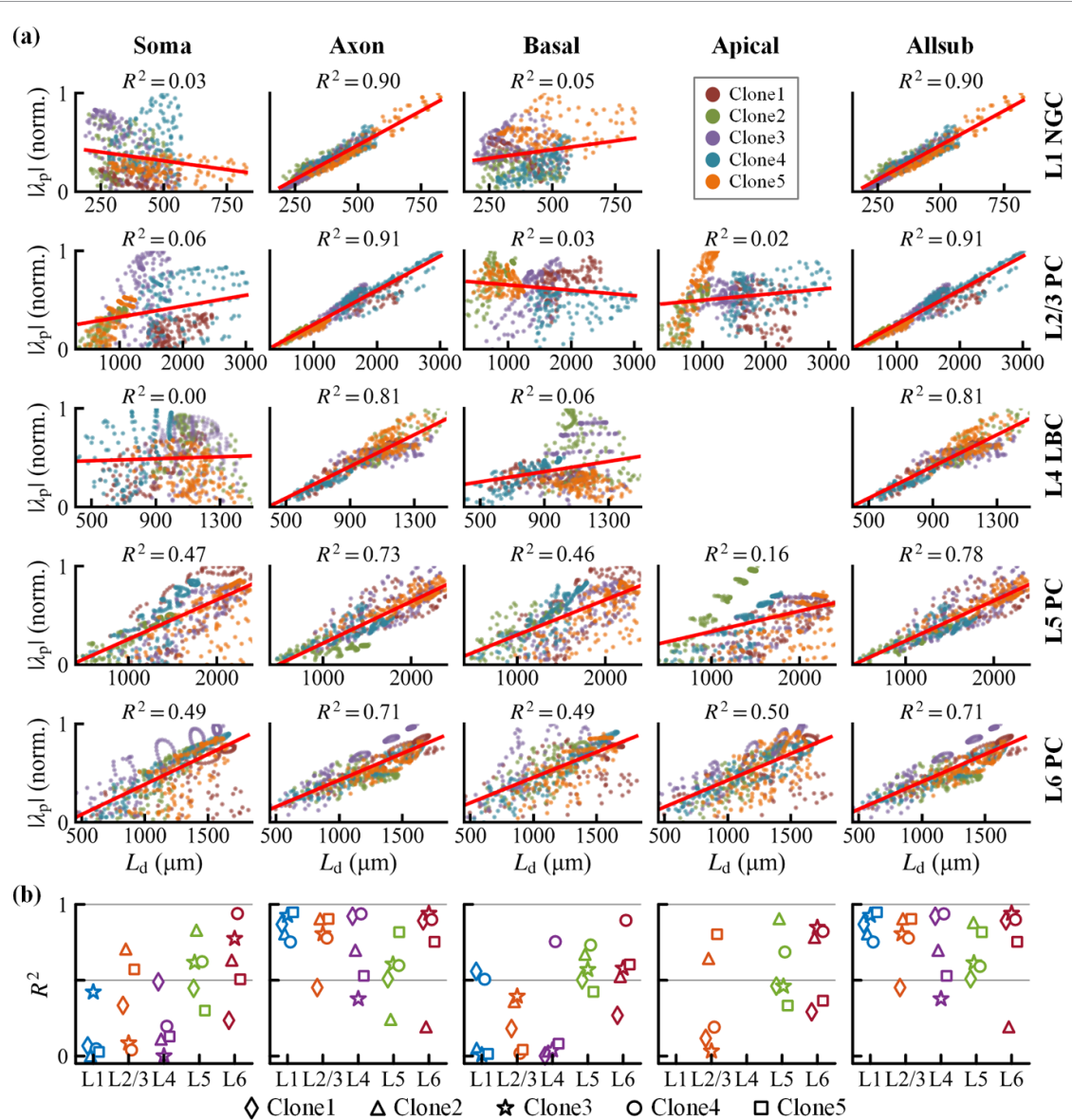


Figure 7. (a) Correlation between the normalized peak polarization length $|\lambda_p|$ and the effective polarization length L_d in each subcellular element for the 5 clones of each cell type across the full range of possible field directions. Data points of different clones are color-coded, and the red lines denote the linear regressions. (b) Correlation coefficient R^2 in each subcellular element for the 5 clones in the same cell type. Each clone indicated by different geometries.

in the apical dendrites of L5 and L6 PCs. Moreover, L4 inhibitory dynamics slightly increases the polarization phase in each subcellular element of pyramidal cells, with little effect on the polarization phase of L1 NGCs (figure S6).

Above analyses demonstrate that the cell morphology and biophysics both are crucial factors in determining the membrane polarization in response to weak oscillating EFs, indicating that the neuronal intrinsic property is one of the major sources of the variability of tACS cellular effects.

4. Discussion

We use a set of neocortical neuron models with realistic morphologies and detailed biophysics to examine the membrane polarization across cell types

and subcellular elements under weak oscillating EF stimulation. Our results show that the membrane polarization is sensitive to the applied field direction, intensity, and frequency, and such field sensitivity varies between cell types and subcellular elements. We further quantify the effects of effective length and excitatory/inhibitory ion dynamics on above frequency-dependent polarization, and the results highlight the crucial role of cell morphology and biophysics in responsiveness to oscillating EFs. These findings contribute to the understanding of complex polarization patterns across cell types as well as subcellular elements, which should be considered when understanding the tACS cellular effects.

Earlier studies [16, 18, 22] have identified the crucial role of cell morphology in determining the neural response to tACS. Aspart *et al* find that the bending

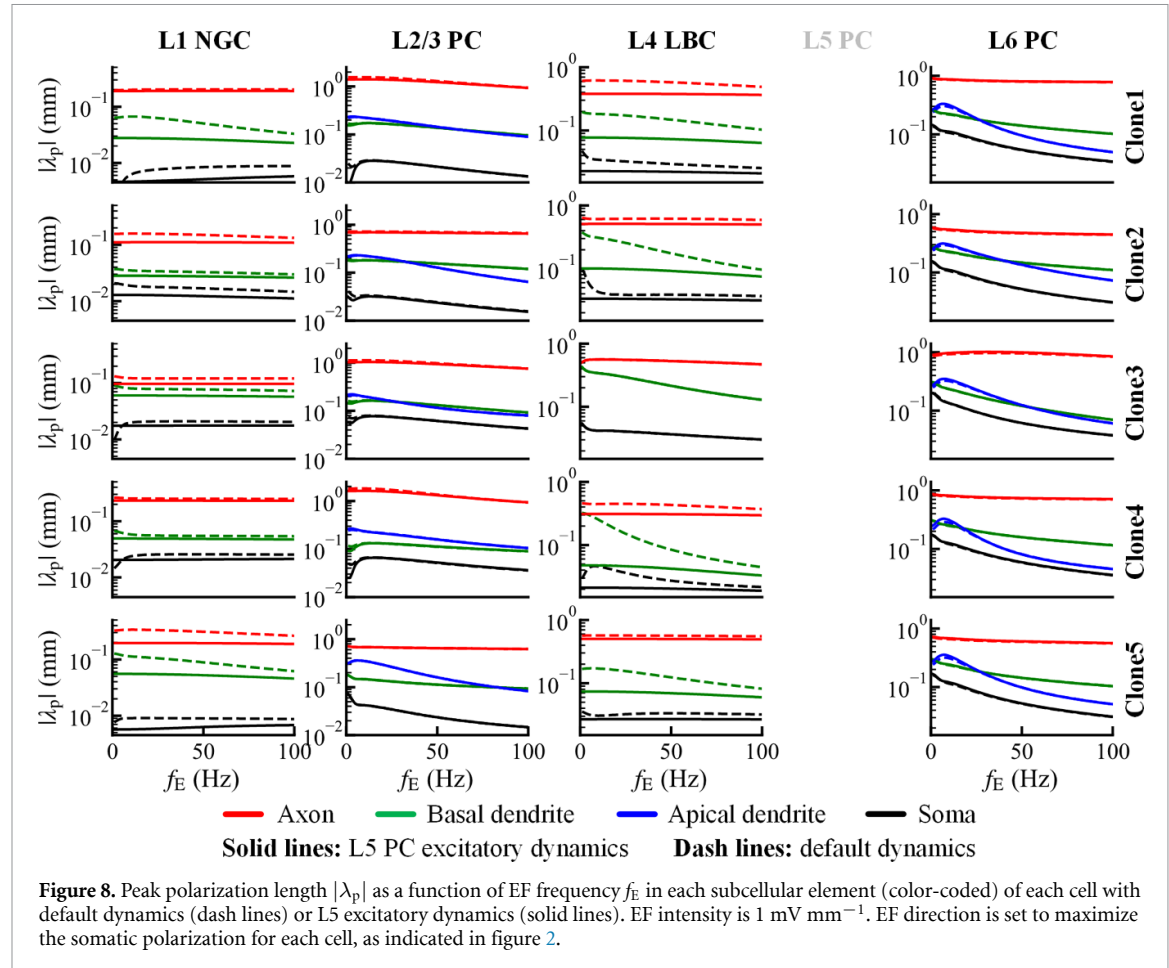


Figure 8. Peak polarization length $|\lambda_p|$ as a function of EF frequency f_E in each subcellular element (color-coded) of each cell with default dynamics (dash lines) or L5 excitatory dynamics (solid lines). EF intensity is 1 mV mm^{-1} . EF direction is set to maximize the somatic polarization for each cell, as indicated in figure 2.

angle and branches of basal dendrites affect the frequency-dependent polarization in different compartments using passive cable models [18]. Huang *et al* find that the proportion of membrane area occupied by somatic compartment modulates the frequency-dependent polarization length and phase in the soma and dendrite using two-compartment models [16]. These two studies are based on the simplified models without considering realistic cell morphologies. Furthermore, Tran *et al* use a set of morphologically realistic models to examine the influence of cell morphology on tACS cellular effects at a given frequency, i.e. 10 Hz [22]. They quantify the morphology for each cell by computing the effective length along the field direction. Their results show that the somatic polarization and neural entrainment are positively correlated to the effective length. In fact, the cortical neurons include not only the soma, but also the extended axons and dendrites, which are also polarized by EF stimulation. In particular, a recent study demonstrates that the axonal and dendritic polarizations are higher than the somatic polarization during transcranial direct current stimulation [26]. However, it is not clear how the membrane polarization by tACS varies between subcellular elements and cell types.

In this work, we use a set of morphologically realistic models of neocortical neurons to simulate the cellular response to oscillating EFs. We systematically examine the membrane polarization in the soma, axons, and dendrites with varying field directions, intensities, and frequencies. We find that the membrane polarization is sensitive to the stimulation parameters, especially its frequency. Moreover, such polarization varies between cell types and subcellular elements. Pyramidal cells tend to be more polarized than interneurons. Axons usually experience the highest polarization, followed by the dendrites and soma. These findings emphasize the cell type- and subcellular element-specific polarization to applied oscillating fields, which indicate the crucial role of cell morphology in the neuronal response to tACS.

One major finding of our work is that the membrane polarization strongly depends on the stimulation frequency, and such frequency-dependent polarization varies between cell types and subcellular elements. For pyramidal neurons, the polarization in the soma, axons, and basal dendrites primarily exhibit low-pass filtering properties due to passive membrane properties. Moreover, we observe a visible frequency resonance in the apical dendritic polarization of pyramidal cells, which has been ever found in experiment

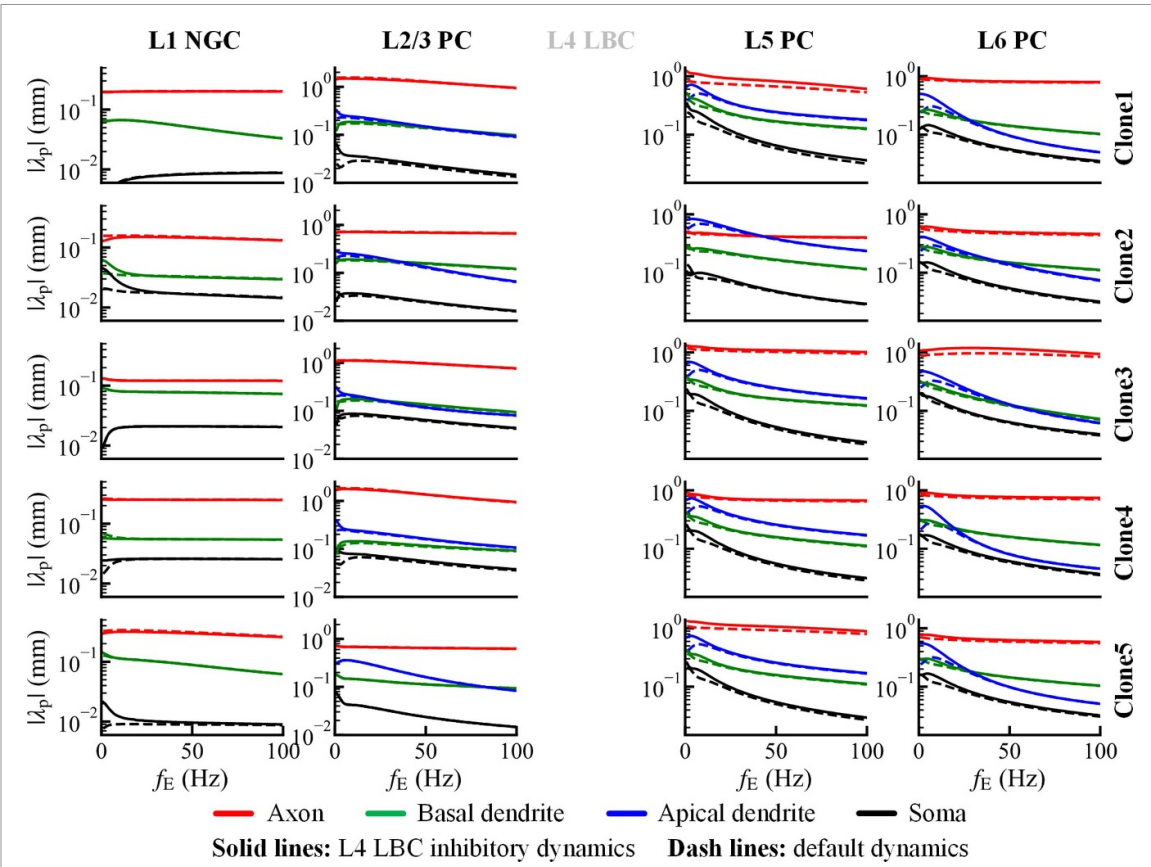


Figure 9. Peak polarization length $|\lambda_p|$ as a function of EF frequency f_E in each subcellular element (color-coded) of each cell with default dynamics (dash lines) or L4 inhibitory dynamics (solid lines). EF intensity is 1 mV mm^{-1} . EF direction is set to maximize the somatic polarization for each cell, as indicated in figure 2.

[28] and modeling studies [15, 16, 18]. This frequency resonance is related to the hyperpolarization-activated cation current in the apical dendrites [15, 16, 18]. Some resonant currents also result in the dendritic frequency resonance [29, 30]. Nevertheless, each subcellular element of interneurons exhibits rather complex filtering properties, including low-pass, band-pass and high-pass filtering. In addition, the polarization phase of cortical neurons is also frequency-dependent, which exhibits high-pass filtering properties.

Experimental studies [3, 13] have identified that tACS can modulate the spike timing of single neurons, and such modulation depends on the stimulation intensity and frequency. In fact, tACS generates a weak oscillating EF in the targeted brain area, which induces transient membrane de- and hyperpolarization periodically. This subthreshold polarization is unable to make a neuron reach its spike threshold and fire an action potential without additional inputs. In contrast, the subthreshold dynamics of membrane voltage affects the spike threshold [31] and spike timing [32]. The field-induced membrane polarization modulates ongoing activity by facilitating or suppressing neuron firing [14]. Earlier review [33] also emphasizes that small membrane polarization induced by tACS leads to changes in spike

rate and spike timing. Our results show that pyramidal cells experience the higher somatic polarization than interneurons, which suggests that tACS has a stronger effect on the spiking activity of pyramidal neurons. Moreover, the somatic polarization in most cells exhibits low-pass filtering properties, indicating that low-frequency tACS results in stronger effects on neural dynamics. Furthermore, Lafon *et al* identify that the weak EF not only changes the spiking output in the soma, but also modulates the synaptic input in the dendrites [34]. Our results show that axons experience the highest polarization. This subthreshold presynaptic de- or hyperpolarization modulates the amplitude of synaptic release [35], thereby influencing the postsynaptic input. Dendritic polarization affects the synaptic input and its propagation, while somatic polarization modulates the spiking output. Therefore, these findings should be considered when understanding how tACS alters the input/output function of cortical neurons in human.

The tACS protocol includes the setting of electrode configuration (size, position) and stimulation waveform (frequency, intensity, and duration) [36, 37], which determine the EF generated in the targeted brain area that interacts with the neural dynamics. There is evidence that the effects of tACS on brain function or behavior in human are specific

to a particular stimulation protocol [36–40]. Even at the cellular level, experimental study indicates that the tACS effects on neural activity are dependent on the stimulation dose [13]. In this work, stimulation intensity ranges between 0.1 mV mm^{-1} and 3 mV mm^{-1} , and stimulation frequency ranges between 1 Hz and 100 Hz. These ranges involve the intensity and frequency of the generating EFs in human cortex by traditional tACS [41, 42]. Moreover, varying electrode position results in changes in the direction of induced EFs relative to cortical neurons, which is replicated by the full range of possible field orientations in our work.

Our results show that excitatory and inhibitory cells experience the higher polarization at low frequencies ($<60 \text{ Hz}$), which corresponds to the frequency range for practical tACS applications [36, 37], e.g. delta, theta, alpha, beta, and gamma. Earlier study demonstrates that pyramidal cells generate large current dipole moments and contribute significantly to the local field potential (LFP) and electroencephalogram (EEG) signals, due to their preferred orientation perpendicular to the cortex surface [43, 44]. Our results show that pyramidal cells experience the higher polarization than interneurons within considered frequency ranges. Moreover, the polarization in the apical dendrites of pyramidal cells exhibit band-pass filtering properties with resonance frequency ranging between 4 Hz and 12 Hz. These results indicate that theta- or alpha-tACS primarily modulates the neural activity of pyramidal cells, thereby affecting the relevant rhythms of measured LFP or EEG signals. Earlier studies show that tACS effects outlast the duration of stimulation [45, 46], which is related to synaptic plasticity [46–48]. Our results show that the axons and dendrites experience the higher polarization than the soma. Subthreshold axonal polarization modulates the amplitude of synaptic release [35], while dendritic polarization affects the postsynaptic potential [34]. These findings are consistent with previous report that tACS acts on synaptic plasticity [4], which indicates that our results contribute to the understanding of tACS aftereffects. In addition, our results show that pyramidal cells are more sensitive to axial field, while interneurons are sensitive to axial and transverse field. These directional sensitivities suggest that not only stimulation waveform but also electrode position should be considered when understanding the electrophysiological effects of tACS in human. In summary, our results reveal the potential effects of traditional tACS at the cellular level, and could provide insights into the design of rational tACS protocols to some extent.

Our study focuses on the membrane polarization at the cellular level, while the parameter optimization of tACS is usually based on measured EEG or functional magnetic resonance imaging signals [49, 50]. To optimize the macroscale tACS parameters

using the microscale neural mechanisms, we need to relate membrane polarization with spike activity and identify the crucial role of neural spiking in brain oscillations. However, it is challenging to record large-scale neuronal responses simultaneously [44] and denoise the high-amplitude stimulation artifacts [50, 51]. Our model study combined with subject-specific head models and experiments will be an effective method to optimize the tACS parameters to an individual brain, such as the closed-loop framework proposed in the literature [50] for designing personalized transcranial electric stimulation parameters.

Temporal interference (TI) stimulation is a non-invasive neurostimulation technique that utilizes high-frequency (kHz) external EFs to stimulate deep neuronal structures without affecting superficial, off-target structures [52–54]. TI stimulation delivers kHz sinusoidal stimulation to multiple electrodes on the scalp, where small differences in frequency between electrodes results in a low-frequency amplitude-modulated EF in the deep brain area [54]. In fact, neurons are more sensitive to weak sinusoidal EFs at stimulation frequencies below 100 Hz [3, 17] but not evidently to weak kHz field stimulation [17, 33], due to the low-pass filtering properties of neuronal membranes [17, 53]. Therefore, neurons in the deep brain area respond to the low-frequency oscillating envelope rather than to the kHz stimulation. Particularly, computational studies [55, 56] use the morphologically and biophysically realistic models to examine cell response to TI stimulation, and their results demonstrate that the resulting low-frequency envelope with 10 Hz can affect both sub-threshold and firing activity in cortical neurons. In this work, we use the same neuron models to examine the cellular and subcellular polarization to oscillating EFs at low frequencies (1–100 Hz), which includes the frequency range of the amplitude-modulated EF induced by TI stimulation. Therefore, our results should be considered when understanding the cellular effects of TI stimulation, and our approach could be extended to the study of the mechanism of TI stimulation.

There are some limitations in our work. First, even though our model set includes various morphologies spanning all neocortical layers, there is still an immense diversity of cell types in neocortex [23] that are supposed to be systematically studied in the future work. Second, we investigate the cellular response to oscillating EFs in the absence of synaptic inputs. Indeed, neurons receive the synaptic inputs from thousands of presynaptic cells *in vivo* [57] and produce action potentials. The synaptic inputs should be included when understanding how tACS affects the input/output transfer function. Third, we use the uniform oscillating EFs to model the tACS cellular effects. In fact, the exogenous EF generated by non-invasive brain stimulation is non-uniformly distributed at the

cellular level [26, 58], which should be taken into consideration in the future work.

5. Conclusion

We use a set of multi-compartmental, conductance-based neuron models with realistic morphologies and biophysics across all neocortical layers to examine the membrane polarization by tACS. We systematically characterize the subthreshold response to oscillating EFs with varying directions, intensities, and frequencies, and quantify the effects of intrinsic properties on membrane polarization across cell types and subcellular elements. Our results show that the membrane polarization is sensitivity to the direction, intensity, and frequency of oscillating EFs. The polarization length and polarization phase both are highly dependent on field frequency. In general, pyramidal cells experience the higher polarization than interneurons, especially layer 5 and 6 pyramidal cells. Axons usually experience the highest polarization, followed by dendrites, while soma has the lowest polarization. These findings indicate that the frequency-dependent membrane polarization is cell type- and subcellular element-specific. Furthermore, we emphasize the importance of cell morphology and biophysics in responsiveness to electrical stimulation. These results highlight the diverse polarization patterns between cell types and subcellular elements during oscillating EFs, which provide deep insights into the cellular effects of tACS and should be considered when understanding the neural spiking activity by tACS.

Data availability statement

The data that support the findings of this study are openly available at the following URL/DOI: https://github.com/preciousXL/Polarization_By_tACS.

Acknowledgments

This work was supported in part by the National Natural Science Foundation of China under Grant Nos. 62171312 and 62071324.

Conflict of interest

The authors declare that they have no known competing financial interests or personal relationships that could have appeared to influence the work reported in this paper.

ORCID iDs

Xile Wei  <https://orcid.org/0000-0002-9157-0978>
Jiang Wang  <https://orcid.org/0000-0002-2189-8003>

Guosheng Yi  <https://orcid.org/0000-0002-9362-6605>

References

- [1] Antal A and Paulus W 2013 Transcranial alternating current stimulation (tACS) *Front. Hum. Neurosci.* **7** 317
- [2] Polania R, Nitsche M A and Ruff C C 2018 Studying and modifying brain function with non-invasive brain stimulation *Nat. Neurosci.* **21** 174–87
- [3] Krause M R, Vieira P G, Csorba B A, Pilly P K and Pack C C 2019 Transcranial alternating current stimulation entrains single-neuron activity in the primate brain *Proc. Natl Acad. Sci. USA* **116** 5747–55
- [4] Wischniewski M, Alekseichuk I and Opitz A 2023 Neurocognitive, physiological, and biophysical effects of transcranial alternating current stimulation *Trends Cognit. Sci.* **27** 189–205
- [5] Polania R, Moisa M, Opitz A, Grueschow M and Ruff C C 2015 The precision of value-based choices depends causally on fronto-parietal phase coupling *Nat. Commun.* **6** 8090
- [6] Moisa M, Polania R, Grueschow M and Ruff C C 2016 Brain network mechanisms underlying motor enhancement by transcranial entrainment of gamma oscillations *J. Neurosci.* **36** 12053–65
- [7] Reinhart R M G and Nguyen J A 2019 Working memory revived in older adults by synchronizing rhythmic brain circuits *Nat. Neurosci.* **22** 820–7
- [8] Beliaeva V, Savvateev I, Zerbi V and Polania R 2021 Toward integrative approaches to study the causal role of neural oscillations via transcranial electrical stimulation *Nat. Commun.* **12** 2243
- [9] Héroux M E, Loo C K, Taylor J L, Gandevia S C and Wicherts J M 2017 Questionable science and reproducibility in electrical brain stimulation research *PLoS One* **12** e0175635
- [10] Guerra A, Lopez-Alonso V, Chearan B and Suppa A 2020 Solutions for managing variability in non-invasive brain stimulation studies *Neurosci. Lett.* **719** 133332
- [11] Beliaeva V and Polania R 2020 Can low-intensity tACS genuinely entrain neural activity *in vivo?* *Brain Stimul.* **13** 1796–9
- [12] Fröhlich F and McCormick D A 2010 Endogenous electric fields may guide neocortical network activity *Neuron* **67** 129–43
- [13] Johnson L, Alekseichuk I, Krieg J, Doyle A, Yu Y, Vitek J, Johnson M and Opitz A 2020 Dose-dependent effects of transcranial alternating current stimulation on spike timing in awake nonhuman primates *Sci. Adv.* **6** eaaz2747
- [14] Sharma M, Farahani F, Bikson M and Parra L C 2021 Animal studies on the mechanisms of low-intensity transcranial electric stimulation *Transcranial Direct Current Stimulation in Neuropsychiatric Disorders* (Springer) (https://doi.org/10.1007/978-3-030-76136-3_5)
- [15] Toloza E H S, Negahbani E and Frohlich F 2018 Ih interacts with somato-dendritic structure to determine frequency response to weak alternating electric field stimulation *J. Neurophysiol.* **119** 1029–36
- [16] Huang X L, Wang J and Yi G S 2023 Frequency-domain analysis of membrane polarization in two-compartment model neurons with weak alternating electric fields *Cogn. Neurodyn.* (<https://doi.org/10.1007/s11571-023-09980-w>)
- [17] Deans J K, Powell A D and Jefferys J G R 2007 Sensitivity of coherent oscillations in rat hippocampus to AC electric fields *J. Physiol.* **583** 555–65
- [18] Aspart F, Remme M W H and Obermayer K 2018 Differential polarization of cortical pyramidal neuron dendrites through weak extracellular fields *PLoS Comput. Biol.* **14** e1006124
- [19] Aberra A S, Peterchev A V and Grill W M 2018 Biophysically realistic neuron models for simulation of cortical stimulation *J. Neural Eng.* **15** 066023

- [20] Radman T, Ramos R L, Brumberg J C and Bikson M 2009 Role of cortical cell type and morphology in subthreshold and suprathreshold uniform electric field stimulation *in vitro* *Brain Stimul.* **2** 215–28
- [21] Lee S Y, Baftizadeh F, Campagnola L, Jarsky T, Koch C and Anastassiou C A 2023 Cell class-specific electric field entrainment of neural activity *bioRxiv Preprint* <https://doi.org/10.1101/2023.02.14.528526> (posted online 15 February 2023)
- [22] Tran H, Shirinpour S and Opitz A 2022 Effects of transcranial alternating current stimulation on spiking activity in computational models of single neocortical neurons *Neuroimage* **250** 118953
- [23] Markram H *et al* 2015 Reconstruction and simulation of neocortical microcircuitry *Cell* **163** 456–92
- [24] Ramaswamy S *et al* 2015 The neocortical microcircuit collaboration portal: a resource for rat somatosensory cortex *Front. Neural Circuits* **9** 1–14
- [25] Chakraborty D, Truong D Q, Bikson M and Kaphzan H 2018 Neuromodulation of axon terminals *Cereb. Cortex* **28** 2786–94
- [26] Aberra A S, Wang R, Grill W M and Peterchev A V 2023 Multi-scale model of axonal and dendritic polarization by transcranial direct current stimulation in realistic head geometry *Brain Stimul.* **16** 1776–91
- [27] Hines M L and Carnevale N T 1997 The neuron simulation environment *Neural Comput.* **9** 1179–209
- [28] Narayanan R and Johnston D 2007 Long-term potentiation in rat hippocampal neurons is accompanied by spatially widespread changes in intrinsic oscillatory dynamics and excitability *Neuron* **56** 1061–75
- [29] Laudanski J, Torben-Nielsen B, Segev I, Shamma S and Deco G 2014 Spatially distributed dendritic resonance selectively filters synaptic input *PLoS Comput. Biol.* **10** e100375
- [30] Rotstein H G and Nadim F 2014 Frequency preference in two-dimensional neural models: a linear analysis of the interaction between resonant and amplifying currents *J. Comput. Neurosci.* **37** 9–28
- [31] Platkiewicz J, Brette R and Graham L J 2010 A threshold equation for action potential initiation *PLoS Comput. Biol.* **6** e1000850
- [32] Radman T, Parra L and Bikson M 2006 Amplification of small electric fields by neurons; implications for spike timing *Int. Conf. IEEE Engineering in Medicine and Biology Society* pp 4949–52
- [33] Reato D, Rahman A, Bikson M and Parra L C 2013 Effects of weak transcranial alternating current stimulation on brain activity—a review of known mechanisms from animal studies *Front. Hum. Neurosci.* **7** 687
- [34] Lafon B, Rahman A, Bikson M and Parra L C 2018 Direct current stimulation alters neuronal input/output function *Brain Stimul.* **10** 36–45
- [35] Zbili M, Rama S and Debanne D 2016 Dynamic control of neurotransmitter release by presynaptic potential *Front. Cell. Neurosci.* **10** 1–6
- [36] Tavakoli A V and Yun K 2017 Transcranial alternating current stimulation (tACS) mechanisms and protocols *Front. Cell. Neurosci.* **11** 214
- [37] Vogeti S, Boetzel C and Herrmann C S 2022 Entrainment and spike-timing dependent plasticity—a review of proposed mechanisms of transcranial alternating current stimulation *Front. Syst. Neurosci.* **16** 827353
- [38] Wischnewski M, Zerr P and Schutter D J L G 2016 Effects of theta transcranial alternating current stimulation over the frontal cortex on reversal learning *Brain Stimul.* **9** 705–11
- [39] Wischnewski M, Joergensen M L, Compenn B and Schutter D J L G 2020 Frontal beta transcranial alternating current stimulation improves reversal learning *Cereb. Cortex* **30** 3286–95
- [40] Spooner R K and Wilson T W 2023 Spectral specificity of gamma-frequency transcranial alternating current stimulation over motor cortex during sequential movements *Cereb. Cortex* **33** 5347–60
- [41] Huang Y, Liu A A, Lafon B, Friedman D, Dayan M, Wang X, Bikson M, Doyle W K, Devinsky O and Parra L C 2017 Measurements and models of electric fields in the *in vivo* human brain during transcranial electric stimulation *eLife* **6** e35178
- [42] Opitz A *et al* Opitz 2016 Spatiotemporal structure of intracranial electric fields induced by transcranial electric stimulation in humans and nonhuman primates *Sci. Rep.* **6** 31236
- [43] Næss S, Halnes G, Hagen E, Hagler D J, Dale A M, Einevoll G T and Ness T 2021 Biophysically detailed forward modeling of the neural origin of EEG and MEG signals *Neuroimage* **225** 117467
- [44] Munn B R, Müller E J, Medel V, Naismith S L, Lizier J T, Sanders R D and Shine J M 2023 Neuronal connected burst cascades bridge macroscale adaptive signatures across arousal states *Nat. Commun.* **14** 6846
- [45] Kasten F H, Dowsett J and Herrmann C S 2016 Sustained aftereffect of α -tACS last up to 70 min after stimulation *Front. Hum. Neurosci.* **10** 245
- [46] Wischnewski M, Engelhardt M, Salehinejad M A, Schutter D J L G, Kuo M F and Nitsche M A 2019 NMDA receptor-mediated motor cortex plasticity after 20 Hz transcranial alternating current stimulation *Cereb. Cortex* **29** 2924–31
- [47] Pariz A, Trotter D, Hutt A, Lefebvre J and Bush D 2023 Selective control of synaptic plasticity in heterogeneous networks through transcranial alternating current stimulation (TACS) *PLoS Comput. Biol.* **19** e1010736
- [48] Schwab B C, König P and Engel A K 2021 Spike-timing-dependent plasticity can account for connectivity aftereffects of dual-site transcranial alternating current stimulation *Neuroimage* **237** 118179
- [49] Chen L L, Madhavan R, Rapoport B I and Anderson W S 2011 Real-time brain oscillation detection and phase-locked stimulation using autoregressive spectral estimation and time-series forward prediction *IEEE Trans. Biomed. Eng.* **60** 753–62
- [50] Soleimani G *et al* 2023 Closing the loop between brain and electrical stimulation: towards precision neuromodulation treatments *Transl. Psychiatry* **13** 279
- [51] Noury N, Hipp J F and Siegel M 2016 Physiological processes non-linearly affect electrophysiological recordings during transcranial electric stimulation *Neuroimage* **140** 99–109
- [52] Grossman N *et al* 2017 Noninvasive deep brain stimulation via temporally interfering electric fields *Cell* **169** 1029–41
- [53] Mirzakhilili E, Barra B, Capogrosso M and Lempka S F 2020 Biophysics of temporal interference stimulation *Cell Syst.* **11** 557–72
- [54] Esmaeilpour Z, Kronberg G, Reato D, Parra L C and Bikson M 2021 Temporal interference stimulation targets deep brain regions by modulating neural oscillations *Brain Stimul.* **14** 55–65
- [55] Wang B S, Aberra A S, Grill W M and Peterchev A V 2023 Responses of model cortical neurons to temporal interference stimulation and related transcranial alternating current stimulation modalities *J. Neural Eng.* **19** 066047
- [56] Luff C E, Dzialecka P, Acerbo E, Williamson A and Grossman N 2024 Pulse-width modulated temporal interference (PWM-TI) brain stimulation *Brain Stimul.* **17** 92–103
- [57] Rahman A, Lafon B and Bikson M 2015 Multilevel computational models for predicting the cellular effects of noninvasive brain stimulation *Prog. Brain Res.* **222** 25–40
- [58] Anastassiou C A, Montgomery S M, Barahona M, Buzsáki G and Koch C 2010 The effect of spatially inhomogeneous extracellular electric fields on neurons *J. Neurosci.* **30** 1925–36